

基于凹型谐振光栅的高性能光学折射率传感器

包益宁¹, 刘秀红^{1*}, 胡劲华², 韩海燕¹, 朱巧芬¹, 席思星¹, 余九州²

¹河北工程大学数理科学与工程学院, 河北 邯郸 056038;

²河北工程大学信息与电气工程学院, 河北 邯郸 056038

摘要 基于导模共振效应的光栅传感器因具有无需荧光标记、易于集成、能实时检测等优点在生物医学传感领域得到了广泛应用。然而, 该类型传感器存在品质因子和灵敏度相互制约的问题。为此提出一种凹型光栅结构, 也就是在周期性光栅的每一个单元中引入凹型微结构, 增强光场与检测物质的相互作用, 进而提升传感器的品质因数。利用严格耦合波算法设计了器件结构, 分析器件的本征模式, 阐明其物理机理。仿真结果表明, 该器件的品质因数可达到 6562.5。本研究工作将为研制基于微纳结构的高性能集成光学传感器提供研究基础。

关键词 集成光学; 集成光学传感器; 品质因数; 导模共振光栅; 严格耦合波分析

中图分类号 O436

文献标志码 A

doi: 10.3788/CJL202148.0913001

1 引言

近年来, 微纳集成光学传感器被广泛应用于生物探测^[1]、环境检测^[2]、生化分析^[3]等领域。构建微纳集成光学传感器常用的功能单元有微环谐振器^[4]、光子晶体波导^[5]、导模共振光栅^[6]等。按照入射光与传感器芯片的耦合形式, 功能单元一般可以分成侧面耦合型和垂直耦合型两类。微环谐振器和光子晶体波导一般采用侧面耦合入光的形式, 与光源直接耦合时模场失配较大, 另外微环谐振器存在模式体积大、品质因数小等缺点, 限制了该类器件在光学传感领域的应用。相比光栅结构, 光子晶体波导需要精准设计微纳结构和严格控制工艺误差。因此, 导模共振光栅结构相比其他两类器件是一种较好的选择, 易于与入射光源垂直耦合。通过设计光栅单元结构, 可以有效调控光栅的漏模谐振, 增强漏模光场与检测液体的相互作用, 提升光学传感器性能指标。

1993 年, Wang 等^[7]发现了周期性波导光栅的导模共振效应。该效应指入射光波与光栅的导模相位匹配时, 由于光栅结构的调制作用, 输出光谱会出

现尖锐的谐振峰。导模共振光栅结构的谐振波长与待测液体的折射率有关, 待测液体折射率变化会引起谐振峰波长漂移, 进而感知待测液体折射率变化, 实现折射率传感。Szeghalmi 等^[8]设计了适用于可见光波段的氧化钛导模共振折射率传感器, 器件的灵敏度为 200 nm/RIU (RIU 为折射率单元), 品质因数(FOM)为 1000。Wang 等^[9]设计了一种基于耦合光栅的导模共振传感器, 用以气体检测, 其灵敏度为 748 nm/RIU, 而 FOM 仅为 374。Wang 等^[10]利用表面离子共振和导模共振的杂化, 设计了一种混合型导模共振折射率传感器, 灵敏度为 1087 nm/RIU, FOM 仅为 23。普通的导模共振光栅折射率传感器的 FOM 较低, 难以实现高品质因数的光学折射率传感。

为了更好地提升导模共振光栅折射率传感器的 FOM, 本文在普通双层导模共振光栅的基础上引入凹型空隙, 提出了一种新型的凹型导模共振光栅折射率传感器。通过严格耦合波分析(RCWA)算法^[11-12]设计了器件结构, 分析了光栅结构参数变化对传感器性能的影响, 在此基础上, 利用有限元算法分析凹型光栅的本征模式, 阐明了品质因数增强的机理。

收稿日期: 2020-09-04; 修回日期: 2020-10-10; 录用日期: 2020-11-11

基金项目: 国家自然科学基金(61905060, 11904073, 21976049)、河北省自然科学基金(F2019402063, F2019402351)、河北省教育厅青年拔尖项目(BJ2020028)

*E-mail: liuxihong@hebeu.edu.cn

2 器件的结构与原理

基于导模共振光栅的传感器一般有三个重要的性能指标,即灵敏度、品质因子和品质因数。

传感器灵敏度(S)的定义为谐振峰波长漂移量($\Delta\lambda$)与待测液体折射率变化量(Δn_c)的比值,即

$$S = \frac{\Delta\lambda}{\Delta n_c} \quad (1)$$

传感器品质因子(Q)的定义为谐振峰波长(λ_{res})与光谱半峰全宽(FWHM)的比值,即

$$Q = \frac{\lambda_{res}}{\tau_{FWHM}} \quad (2)$$

为了提高品质因子 Q ,要求光谱线宽较小。传感器的 FOM 可以综合衡量传感器的灵敏度和品质因子,表达式^[13]为

$$R_{FOM} = \frac{SQ}{\lambda_{res}} \quad (3)$$

为了实现高 FOM 的集成光栅传感器,需要同时提高灵敏度和品质因子。然而,该类传感器存在灵敏度 S 与品质因子 Q 相互制约的问题。具体物理解释为:要实现高灵敏度的光栅传感器,需要光栅中更多的光场泄漏到具有低折射率的待检测液体中;同时,要获得高品质因子的光栅传感器,需要提升光栅对漏模光场的束缚能力,使光场集中在高折射率的光栅区域。因此,具有单一周期性的导模共振光栅由于结构的对称性,难以同时实现高灵敏度和高品质因子的光学传感。所以普通的导模共振光栅型传感器的 FOM 一般较低^[14-15]。

为了解决这一问题,本文提出了一种双层凹型谐振光栅折射率传感器,也就是在普通的周期性光栅单元中引入凹型微结构,增强光栅对光场的束缚能力,同时也增强输出光场与覆盖层待检测液体的

相互作用。该传感器由覆盖层待测液体、凹型氮化硅光栅层(折射率 $n_1=2$)、氮化硅平板波导层、氧化硅衬底(折射率 $n_2=1.45$)组成,器件结构如图 1 所示。光栅层厚度、波导层厚度、光栅周期、占空比分别用 D_g 、 D_s 、 Λ 、 f_a 来表示,光栅表面设计一个矩形的凹槽,凹槽上表面的中点与光栅脊上表面中点重合。凹槽的深度为 D_r ,凹槽的宽度和左右子光栅的宽度分别为 $f_b \times f_a \times \Lambda$ 、 $f_c \times f_a \times \Lambda$,其中 f_b 、 f_c 为凹槽和子光栅的宽度系数且 $f_b + 2f_c = 1$ 。

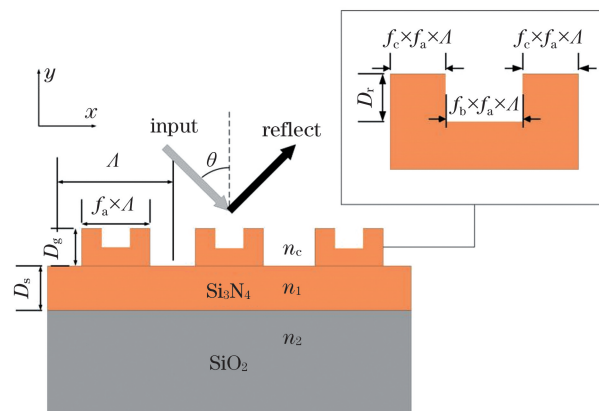


图 1 凹型谐振光栅的结构示意图

Fig. 1 Schematic of concave resonant grating

3 结果与讨论

为了研究凹型导模共振光栅反射光谱特性,令器件结构参数为:光栅层厚度 $D_g=120$ nm,波导层厚度 $D_s=180$ nm,光栅周期 $\Lambda=460$ nm,占空比 $f_a=0.85$,宽度系数 $f_b=0.5$, f_c 为 0.25,覆盖层待检测液体的折射率 $n_c=1.331$ 。以 TM 偏振光作为入射光源,选择入射角度为 15° 。利用 RCWA 算法模拟器件的反射光谱,仿真结果如图 2(a)所示,器件的反射光谱线宽仅为 0.03 nm,谐振波长为

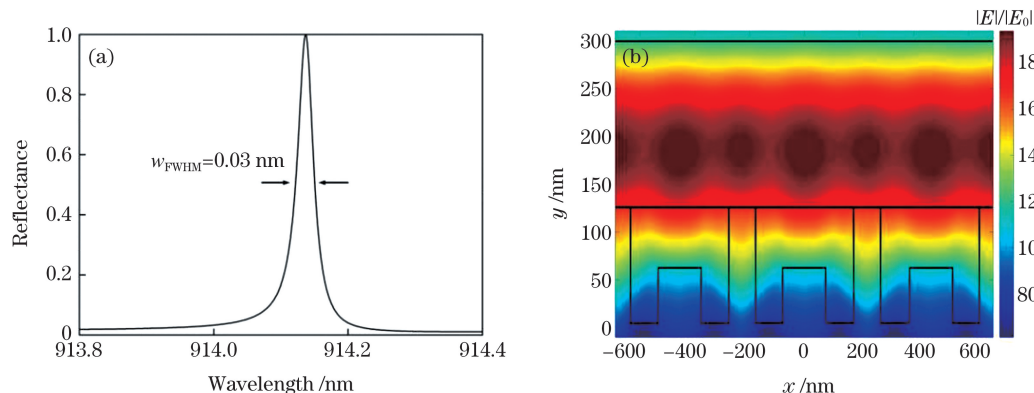


图 2 凹型光栅的反射光谱与谐振峰下的电场分布。(a)仿真的反射光谱;(b)在谐振波长下的电场分布

Fig. 2 Reflection spectrum of concave grating and electric field distribution at resonant wavelength.

(a) Simulated reflection spectrum; (b) electric field distribution at resonance wavelength

914.14 nm。为了更直观地理解该现象,给出结构在谐振波长下的磁场强度分布,如图 2(b)所示。入射场强度 E_0 设为 1,其绝对值 $|E|/|E_0|$ 为磁场强度。结果表明,在谐振波长处,波导区域和光栅区域存在明显的场强增强。

为了阐明光栅结构深度 D_r 变化对光学谐振的调控机理,将光栅视为一个单模的谐振器,以一个周期单元为研究对象,左右边界采用 Floquet 边界周期边界条件,上下采用散射边界条件。选择覆盖层待检测液体折射率为 1.331,利用有限元算法计算光栅参数 $D_r=30,60,90$ nm 时的本征模 $N=N_{real}-iN_{imag}$,其中 N_{real} 为实部, N_{imag} 为虚部^[14],本征值的变化如表 1 所示。

表 1 不同空隙槽深度下的 TM 本征模式的本征值
Table 1 Eigenvalues of TM eigenmodes for different D_r

D_r/nm	N
30	$2.0210 \times 10^{15} - 9.754 \times 10^{10} i$
60	$2.0431 \times 10^{15} - 2.262 \times 10^{10} i$
90	$2.0649 \times 10^{15} - 1.152 \times 10^{11} i$

该光学谐振器的谐振角频率和品质因子^[16]可以表示为

$$\begin{cases} \omega_0 = N_{real} \\ Q = N_{real} / 2N_{imag} \end{cases} \quad (4)$$

可以发现 D_r 由 30 nm 变化至 90 nm 时,根据(4)式可以看出,本征值中实部增大表示谐振波长出现蓝移,品质因子随虚部变化先增加后降低。为了进一步验证本征值分析的结果,采用 RCWA 算法分析上述三种结构的反射光谱,结果如图 3 所示,当 D_r 为 30,60,90 nm 时反射光谱的 FWHM 分别为

0.2,0.03,0.12 nm。可以发现:随着光栅结构参数 D_r 的增加,光谱的谐振波长向短波长方向移动,FWHM 先减小后增加;当 $D_r=60$ nm 时,FWHM 最小。光栅结构参数 D_r 变化可以实现对反射光谱线宽的调控。

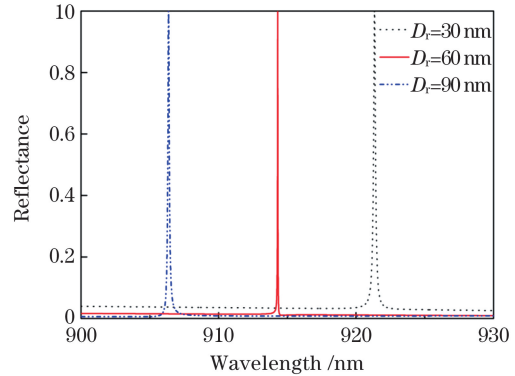


图 3 不同凹槽深度下的反射光谱

Fig. 3 Reflection spectra under different groove depths

当待检测液体折射率由 1.331 变化至 1.339 时,计算出不同 D_r 所对应的传感器的灵敏度,如图 4(a)所示。仿真结果表明,随着 D_r 增大,光栅层处的光场更多地与低折射率的待检测液体相互作用,传感器的灵敏度逐渐提高,但提高程度不显著,根据(3)式,此时 FOM 主要受 FWHM 影响。进一步计算出不同 D_r 下的 FWHM,如图 4(b)所示。结果表明:随着 D_r 增加,FWHM 呈现先减后增的趋势;当 $D_r=60$ nm 时,FWHM 最小为 0.03 nm,这与表 1 中本征值分析的结果吻合。由此可以说明,通过改变光栅的结构参数 D_r ,光栅的本征模式中的本征值发生变化,进一步调控了反射光谱的线宽。综合考虑灵敏度与 FWHM 的变化,选择 $D_r=60$ nm。

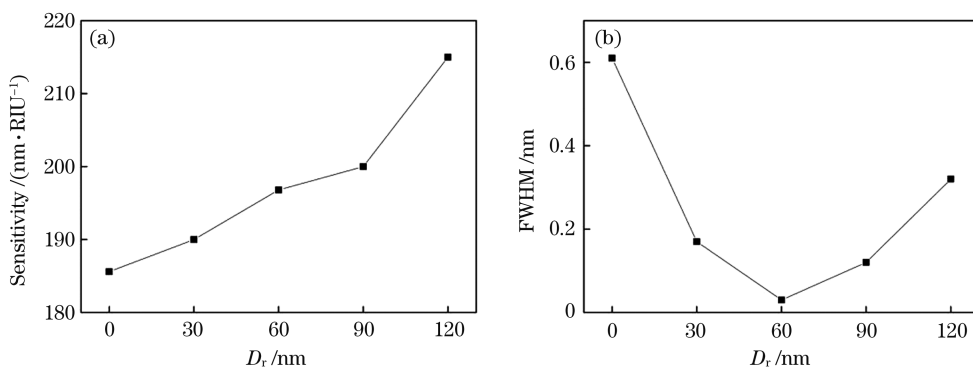


图 4 D_r 不同时结构的灵敏度和光谱线宽。(a)灵敏度;(b)半峰全宽

Fig. 4 Sensitivity and FWHM of the structure under different D_r . (a) Sensitivity; (b) FWHM

进一步研究了凹型结构的宽度变化(不同 f_b)对传感器的灵敏度和光谱线宽的影响。当 $D_r=60$ nm 时,不同 f_b 下,光谱的灵敏度变化曲线如

图 5(a)所示,灵敏度呈现逐渐增加的趋势,但是随着 f_b 从 0.1 增长至 0.9,灵敏度仅仅从 190 nm/RIU 增加至 197.5 nm/RIU, f_b 对灵敏度的影响有限。此

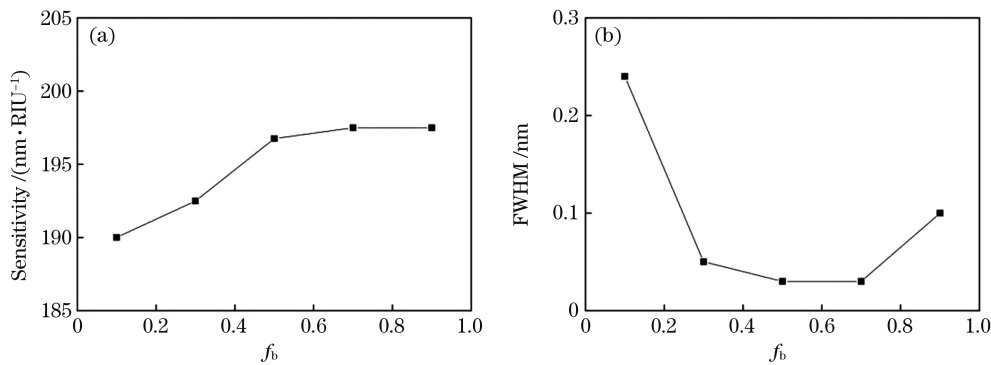


图 5 不同宽度系数时结构的灵敏度和光谱线宽。(a)灵敏度;(b)光谱线宽

Fig. 5 Sensitivity and FWHM of the structure under different width coefficients. (a) Sensitivity; (b) FWHM

时结构的 FOM 主要受 FWHM 影响。利用反射光谱拟合计算得到不同 f_b 下的 FWHM,如图 5(b)所示。随着 f_b 的增大,FWHM 快速减小,从 0.24 nm 减小至 0.03 nm,然后趋于缓和,随着 f_b 继续增大,FWHM 再次增大。

利用有限元算法计算 $f_b = 0.1, 0.3, 0.5$ 时的本征模的本征值,用以阐明 FWHM 在这条件下快速减小的物理机理,如表 2 所示。谐振波长随着 f_b 的增加逐渐向短波长方向移动,在 f_b 从 0.1 变化至 0.3 时,品质因子增大程度明显。以上分析结果进一步验证了图 5(b)的结论。因此选择 $f_b = 0.5$ 。

表 2 不同宽度系数下 TM 本征模的本征值

Table 2 Eigenvalues of TM eigenmodes for different f_b

f_b	N
0.1	$2.0096 \times 10^{15} - 1.515 \times 10^{11} i$
0.3	$2.0268 \times 10^{15} - 2.507 \times 10^{10} i$
0.5	$2.0431 \times 10^{15} - 2.262 \times 10^{10} i$

最后分析了所设计的凹型光栅传感器的性能指标。当待测液体折射率自 1.331 变化至 1.339 时,反射光谱如图 6(a)所示。谐振峰随着待检测物质折射率的增大而红移,FWHM 几乎没有变化。进一步分析谐振峰位置随待检测物质折射率变化的拟合曲线,可以看出谐振波长与折射率之间的变化呈线性关系,如图 6(b)所示,凹型导模共振光栅的折射率灵敏度为 196.875 nm/RIU,FWHM 为 0.03 nm,FOM 为 6562.5。该传感器拥有较高的 FOM,其谐振波长与待测液体折射率之间呈良好的线性关系。

4 结 论

提出了一种基于凹型谐振光栅的折射率传感器。通过改变光栅结构参数,可以调控光栅的本征模式,改变了本征值的大小,达到调控反射光谱线宽

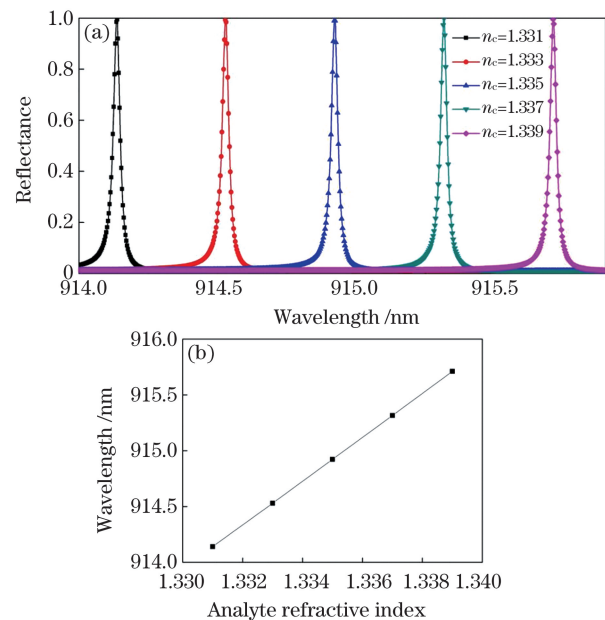


图 6 不同折射率下的反射光谱和反射谐振峰的位置。

(a)仿真的反射光谱;(b)反射谐振峰位置

Fig. 6 Reflection spectra with different refractive index and resonance peak positions. (a) Simulated reflection spectra; (b) reflection resonance peak position

的目的,实现传感器的性能指标的优化。理论仿真结果表明,传感器的灵敏度为 196.875 nm/RIU,FWHM 为 0.03 nm,FOM 值为 6562.5。本研究工作作为新型光栅传感器的设计提供了参考。

参 考 文 献

- [1] Guo L W, Ma J Y. High-sensitive biosensor based on GMR in self-suspended grating[J]. Acta Photonica Sinica, 2012, 41(12): 1483-1487.
郭凌伟, 麻健勇. 基于导模共振效应的自支撑超灵敏生物探测器[J]. 光子学报, 2012, 41(12): 1483-1487.
- [2] Sader E, Sayyed-Ahmad A. Design of an optical water pollution sensor using a single-layer guided-

- mode resonance filter[J]. *Photonic Sensors*, 2013, 3(3): 224-230.
- [3] Cunningham B, Li P, Lin B, et al. Colorimetric resonant reflection as a direct biochemical assay technique[J]. *Sensors and Actuators B: Chemical*, 2002, 81(2/3): 316-328.
- [4] Hiltunen M, Hiltunen J, Stenberg P, et al. Polymeric slot waveguide at visible wavelength[J]. *Optics Letters*, 2012, 37(21): 4449-4451.
- [5] Lu A J, Bai Z C, Xiao W, et al. Design and research of biosensor characteristics based on grating waveguide angle modulation with MEMS micro-mirror[J]. *Chinese Journal of Lasers*, 2016, 43(4): 0414001.
陆安江, 白忠臣, 肖伟, 等. 基于 MEMS 微镜的光栅波导角度调制生物传感器设计与研究[J]. *中国激光*, 2016, 43(4): 0414001.
- [6] Lan G L, Zhang S, Zhang H, et al. High-performance refractive index sensor based on guided-mode resonance in all-dielectric nano-silt array[J]. *Physics Letters A*, 2019, 383(13): 1478-1482.
- [7] Wang S S, Magnusson R. Theory and applications of guided-mode resonance filters[J]. *Applied Optics*, 1993, 32(14): 2606-2613.
- [8] Szeghalmi A, Kley E B, Knez M. Theoretical and experimental analysis of the sensitivity of guided mode resonance sensors[J]. *The Journal of Physical Chemistry C*, 2010, 114(49): 21150-21157.
- [9] Wang L, Sang T, Li J L, et al. High-sensitive transmission type of gas sensor based on guided-mode resonance in coupled gratings[J]. *Journal of Modern Optics*, 2018, 65(13): 1601-1608.
- [10] Wang L, Sang T, Gao J, et al. High-performance sensor achieved by hybrid guide-mode resonance/surface plasmon resonance platform[J]. *Applied Optics*, 2018, 57(25): 7338-7343.
- [11] Moharam M G, Grann E B, Pommet D A, et al. Formulation for stable and efficient implementation of the rigorous coupled-wave analysis of binary gratings[J]. *Journal of the Optical Society of America A*, 1995, 12(5): 1068-1076.
- [12] Moharam M G, Gaylord T K, Pommet D A, et al. Stable implementation of the rigorous coupled-wave analysis for surface-relief gratings: enhanced transmittance matrix approach[J]. *Journal of the Optical Society of America A*, 1995, 12(5): 1077-1086.
- [13] Mayer K M, Hafner J H. Localized surface plasmon resonance sensors[J]. *Chemical Reviews*, 2011, 111(6): 3828-3857.
- [14] Hu J H, Liu X H, Zhao J J, et al. Investigation of Fano resonance in compound resonant waveguide gratings for optical sensing[J]. *Chinese Optics Letters*, 2017, 15(3): 030502.
- [15] Zhou Y, Li X, Li S, et al. Symmetric guided-mode resonance sensors in aqueous media with ultrahigh figure of merit[J]. *Optics Express*, 2019, 27(24): 34788-34802.
- [16] Hu J H, Huang Y Q, Ren X M, et al. Modeling of Fano resonance in high-contrast resonant grating structures[J]. *Chinese Physics Letters*, 2014, 31(6): 064205.

High-Performance Optical Refractive Index Sensor Based on Concave Resonant Grating

Bao Yining¹, Liu Xiuhong^{1*}, Hu Jinhua², Han Haiyan¹, Zhu Qiaofen¹, Xi Sixing¹, Yu Jiuzhou²

¹ School of Mathematics and Physics Science and Engineering, Hebei University of Engineering, Handan, Hebei 056038, China;

² School of Information and Electrical Engineering, Hebei University of Engineering, Handan, Hebei 056038, China

Abstract

Objective High-performance micro-nano integrated optical sensors are widely used for various applications including biomedical sensing. These sensors have several advantages, such as no need of fluorescent labeling, ease of integration, and real-time detection capability. Integrated optical sensors usually include several fundamental components: micro-ring waveguide resonator, photonic crystal waveguide, and guided mode resonance (GMR) grating. Design and implementation of integrated sensors with high figure of merit (FOM) in waveguide-type resonators seem to be complicated due to relatively higher mode volume and mode mismatch. Leaky resonant grating mode can be excited with an input light-wave under certain conditions. The major problem is a trade-off between the

quality factor (Q) and sensitivity (S) of optical biosensors integrated with resonant gratings. To tackle this problem, we designed and implemented concave grating micro-structure. The structure was introduced in each unit of periodic gratings and allowed to enhance interaction between light field and test liquid. Moreover, it improved the quality factor and had no negative effect on sensitivity. Thus, a high-performance integrated sensor with high FOM was obtained using concave resonant grating.

Methods In this study, the proposed integrated sensor was composed of Si_3N_4 grating and SiO_2 layer (Fig. 1). In order to design this structure, we calculated transmission spectrum of the concave resonant grating using rigorous coupled-wave analysis (RCWA) algorithm. Both reflection spectrum of concave grating and distribution of electric field at resonance were observed (Fig. 2). To clarify resonant mechanism of the structure, we investigated its single unit using finite element method (FEM). According to the simulation results, the eigenmode of the structure varied with depth D_r . The sensitivity and full width at half maximum (FWHM) of the structure were both described as the functions of D_r . Eigen mode numerical values agreed well with the RCWA results. Additionally, we analyzed the relationship between other structural parameters (e.g., grating depth D_r and groove width coefficient f_b).

Results and Discussions Reflection spectrum and electric field distribution at resonant wavelength were obtained using RCWA algorithm (Fig. 2). Simulation results demonstrated that optical resonance was significantly enhanced with concave resonant grating structure. In particular, sharp resonant peak was observed (Fig. 2a). To clarify resonant mechanism of proposed structure with different depth D_r and groove width coefficient f_b , we calculated its eigen mode using FEM (Table 1 and Table 2). Interestingly, we found that the eigenvalue changed with the increase of D_r and width coefficient f_b . By these means, resonant wavelength and Q -factor for each mode can be easily restored. Thus, we can predict the characteristics of the transmission spectra with the change of critical parameters such as the depth and width of grating groove. We further optimized FOM of the proposed sensor using RCWA algorithm. We found that the resonant wavelength also followed blue shift trend as the groove width increased. At the same time, groove depth optimal value was found at 60 nm (Fig. 3 and Fig. 4). In addition, we used the same method to study optical spectra when varying width coefficients f_b (Fig. 5). As a result, ultra-high FOM can be achieved at 6562.5, while the sensitivity of the concave GMR is kept at 196.875 nm/RIU.

Conclusions A new-type refractive index sensor based on concave resonant grating has been developed. The concave micro-structure is used to enhance the interaction between optical field and cover grating structure. When introduced in unit cell, it allows optimization FOM. Integrated sensor has been optimized using rigorous coupled-wave analysis. The physical mechanism can be easily understood from calculated eigen mode of the resonant structure. As a result, the ultra-high FOM can be achieved. This provides a basis for the development of high-performance optical sensors integrated with micro-nano structure.

Key words integrated optics; integrated optical sensor; figure of merit; guided mode resonance grating; rigorous coupled wave analysis

OCIS codes 130.6010; 050.6624; 050.2770